Vol. 76: 145–160, 2018
https://doi.org/10.3354/cr01530

CLIMATE RESEARCH
Clim Res

Published online October 10

Detection and attribution of climate change signals in South India maximum and minimum temperatures

P. Sonali[1,*], Ravi S. Nanjundiah[1,2], D. Nagesh Kumar[1,3]

[1]Divecha Centre for Climate Change, Indian Institute of Science, Bangalore 560012, India
[2]Centre for Atmospheric and Oceanic Sciences, Indian Institute of Science, Bangalore 560012, India
[3]Department of Civil Engineering, Indian Institute of Science, Bangalore 560012, India

ABSTRACT: South India has seen significant changes in climate. Previous studies have shown that the southern part of India is more susceptible to effects of climate change than the rest of the country. We performed a rigorous climate model-based detection and attribution analysis to determine the root cause of the recent changes in climate over South India using fingerprint analysis. A modified Mann-Kendall test signalized non-stationariness in maximum and minimum temperatures (T_{max} and T_{min}) in most seasons during the period 1950–2012. The diminishing cloud cover trend may have induced significant changes in temperature during the considered time period. Significant downward trends in relative humidity during most seasons could be evidence of the recent significant warming. The observed seasonal T_{max} and T_{min} change patterns are strongly associated with the El Niño Southern Oscillation. Significant positive associations between South India temperatures and the Niño3.4 index were found in all seasons. The fingerprint approach indicated that the natural internal variability obtained from 14 climate model control simulations could not explain these significant changes in T_{max} (post-monsoon) and T_{min} (pre-monsoon and monsoon) in South India. Moreover, an experiment simulating natural external forcings (solar and volcanic) did not coincide with the observed signal strength. The dominant external factors leading to climate change are greenhouse gases, and their impact is eminent compared to other factors such as land use change and anthropogenic aerosols. Anthropogenic signals are identifiable in observed changes in T_{max} and T_{min} of South India, and these changes can be explained only when anthropogenic forcing is involved.

KEY WORDS: Detection · Attribution · Climate change · South India · Temperature · CMIP5 models · Fingerprint · Signal strength

1. INTRODUCTION

Human activities are among the main contributors to the current climate change. Being a rapidly developing country which is already in a state of water stress, India is experiencing adverse effects of climate change due to growing industrialization and urbanization in recent decades. Large swaths of South India (specifically the interior peninsula) are drought prone because of their geo-climatic setting, high rate of evapotranspiration and intensive use of ground water. The climate of South India is highly diversified, as this area is bounded by the Indian Ocean, Arabian Sea and Bay of Bengal on 3 sides. Moreover, 2 mountain ranges, viz. the Eastern and Western Ghats, and highly arid regions such as north Karnataka (the most arid region in South Asia outside of the Thar Desert), Telangana, and the Rayalaseema region of Andhra Pradesh are also part of this area. Major states (Karnataka, Kerala, Tamil

*Corresponding author: iisc.sonali@gmail.com

Nadu, Andhra Pradesh) and most of the urban areas of India (Chennai, Bengaluru, Hyderabad, Coimbatore, Kochi and Visakhapatnam) are located in South India. Extreme rainfall events which occurred in recent decades in Hyderabad and Chennai (total population of around 18 million) caused huge socio-economic losses (Guhathakurta et al. 2011). This region also experiences frequent high-temperature events during the summer season.

The frequency of hot days has increased significantly over southern parts of India (Kothawale et al. 2010). Singh & Kumar (2015) presented a bottom-up probabilistic Budyko framework to assess the availability of fresh water over all of India and intimated that southern India is more vulnerable to climate change (with a decrease of 25% in fresh water and 10% in precipitation) compared to the northwestern and central parts of India. Kumar et al. (2016) observed that the impact of extreme temperature is higher along the west and east coast respectively during summer and winter seasons (the west and east coast do not exactly represent temperature-homogenous regions). Higher average suicide rates have been recorded among farmers in southern states of India because of the increases in crop-damaging temperatures (Carleton 2017). Therefore, it is crucial to understand the background information and obtain a scientific basis for climate change in the southern part of India.

Numerous studies have been conducted in the recent past pointing at an alarming condition of global and continental temperature increases (Stocker et al. 2013). The Fifth Assessment Report of the Intergovernmental Panel on Climate Change (IPCC AR5) clearly documents that more than half of the observed increase in global mean surface temperature is mostly due to the increment in anthropogenic greenhouse gas (GHG) concentrations (Bindoff et al. 2013). Diurnal temperature ranges have increased globally (Easterling et al. 1997), including in different parts of India, and the warming trend in India is largely consistent with global change (Rupa Kumar et al. 1994, Kothawale et al. 2010, Rai et al. 2012, Vinnarasi et al. 2017). However, during the last 3 decades of the 20th century, the trend in maximum temperature (T_{max}) has been slightly weaker than the trend in minimum temperature (T_{min}) over India and in all temperature-homogenous regions (Sonali & Nagesh Kumar 2013). Surface temperature is a controlling factor for many hydrological and ecological processes. T_{max} and T_{min} are crucial indicators of climate change impact, and in several ways society and ecosystems are impacted more by T_{max} and T_{min} than by mean temperature (T_{mean}) and extreme events. Most of the climate change impact assessment studies carried out over India have focused on precipitation rather than temperature (Sonali & Nagesh Kumar 2013).

A number of studies have focused on the detection of short-term and long-term changes in hydro-climatological variables; of these, only a few focused on the systematic assessment of detection and attribution of climate change using the fingerprint approach over India (Mondal & Mujumdar 2012, Sonali & Nagesh Kumar 2016a). Detection and attribution analysis is a formal tool to trace the complex phenomena which cause climate change.

'Detection' is defined in IPCC-AR5 as the process of demonstrating change in climate with a defined statistical sense without providing a reason for that change. On the other hand, 'attribution' is defined as the process of evaluating the relative contributions of multiple causal factors to a change in climate with an assigned statistical confidence. A considerable effort has been made towards detection and attribution of observed changes in various measures of climate, such as temperature, precipitation, stream flow, ocean circulation indices, ocean heat content, tropospheric moisture content and specific humidity, at global, continental and regional scales (Bindoff et al. 2013).

Ribes et al. (2009) introduced a new adaptation of the 'optimal fingerprint' approach, termed the 'regularized optimal fingerprint' approach, and implemented it successfully to detect and attribute the changes in global mean surface temperature (Ribes et al. 2013). Stone & Hansen (2016) developed an algorithm for systematic assessment of the detection and attribution of regional anthropogenic climate change based on 'confidence' language, which characterizes the total effects of all contributors.

With the exception of a few studies, detection and attribution of climate change have not been researched extensively in India. Trend detection analysis provides individual variability information (at each grid point), whereas fingerprint-based detection and the attribution approach present combined variability information (Hasselmann 1993, Hidalgo et al. 2009). The fingerprint approach reduces the detection problem to a low dimensional space where the signal (such as human-induced climate change) can be extracted smoothly from noise (e.g. natural climate variability). Apart from the global scale, policy makers are interested and more concerned about regional and local-scale detection and attribution.

Sonali & Nagesh Kumar (2016a) compared spatio-temporal patterns of T_{max} and T_{min} over all of India. They indicated that the detected significant changes

are beyond natural internal variability during the latter half of the 20th century. Cho et al. (2016) performed an attribution study to identify the contribution of different external sources causing massive landslides and extreme floods in Uttarakhand, a northern state of India. They found that the root cause of this rainstorm event was a post-1980 climatic trend. Mondal & Mujumdar (2015) highlighted the difficulties in unequivocal attribution of extreme precipitation changes to human-induced effects. Mondal & Mujumdar (2012) and Chithra & Thampi (2015) performed detection and attribution studies of changes in precipitation and streamflow in different river basins of India using CMIP3 climate model simulation. Lau & Kim (2010) attributed the changes in Indian summer monsoon regional precipitation to aerosol effects.

To date, limited studies have been conducted on the formal detection and attribution of climate change employing CMIP5 models over India (Sonali & Nagesh Kumar 2016a), while none has attempted to attribute the changes in temperature in South India to increases in anthropogenic GHG emissions. Hence, the main objective of the present study was to investigate the detectability, and possible attribution, of climate change effects on T_{max} and T_{min} over South India. Firstly, we analyzed the temporal variation of annual and seasonal T_{max} and T_{min} by using a modified Mann-Kendall approach. Secondly, the analysis was extended further to formally detect and attribute the observed changes in T_{max} and T_{min} to different causative factors by employing the fingerprint approach.

2. OBSERVATIONAL AND MODEL DATA

Climatic characteristics differ significantly over South India (shown in Fig. 1), as it consists of 3 different temperature-homogenous regions, viz. the east coast (EC), west coast (WC) and interior peninsula (IP), as defined by the Indian Institute of Tropical Meteorology (IITM, www.tropmet.res.in).

2.1. Observational data

India Meteorological Department (IMD) (Srivastava et al. 2009) temperature records are insufficient for the considered time period (1950–2012). Hence monthly T_{max} and T_{min} datasets from the latest version of CRU3.22 (at 0.5° × 0.5° resolution) produced by the Climate Research Unit (CRU) of the University of East Anglia (Harris et al. 2014) were used as observational data (as the data set is spatially and temporally complete for the considered period). CRU and IMD temperature datasets agree well (with high correlation) during all months and seasons over most of India except for a few grid points located in the Western Himalaya and northeast regions (Sonali & Nagesh Kumar 2016b). This comparison was done by examining the common period of 2 datasets during all seasons and months. None of the poorly correlated grid points are located in South India. South India is covered by a total of 428 grid points (resolution: 0.5° × 0.5°).

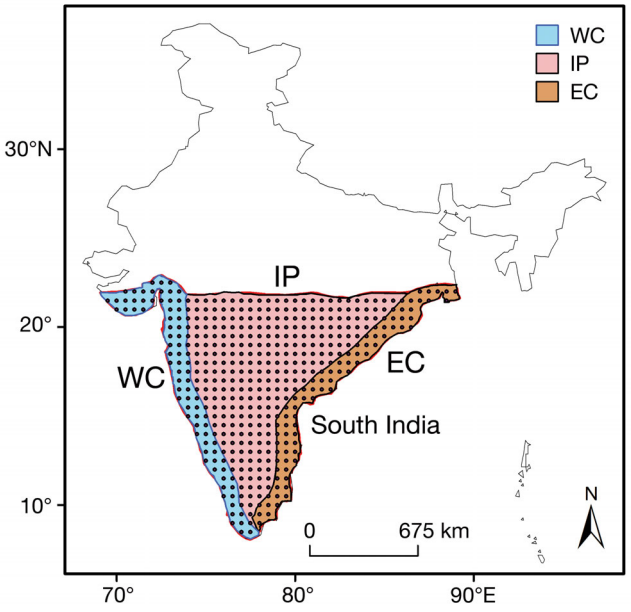

Fig. 1. Study region in South India consisting of 428 grid points and 3 temperature-homogenous regions. WC: west coast; IP: interior peninsula; EC: east coast

2.2. Global model simulation

General circulation models (GCMs) provide simulated patterns of the Earth's climate system with or without forcings. These simulated patterns are contrasted with the actual observations to determine whether the signals of a specific forcing are perceptible. Climate models therefore play a critical role in attribution studies. Previous model evaluation studies have demonstrated that CMIP3 models perform poorly compared to CMIP5 for T_{max}, T_{min} (Raju et al. 2016, Sonali et al. 2017) and precipitation (Mishra et al. 2014) over India. The improved parameterization in terms of aerosol scheme and convection plays a major role in better simulation of precipitation extremes in CMIP5 climate models (Watanabe et al. 2010). Sonali et al. (2017) evaluated the performance of CMIP5 and CMIP3 climate models in their ability

to simulate T_{max} and T_{min} over all of India. A substantial improvement was noted for CMIP5 compared to CMIP3 climate models. Separate shortlisted climate models for T_{max} and T_{min} are considered here, as some climate models could simulate T_{min} better than T_{max}. For model experiments, 9 GCMs each for T_{max} and T_{min} from the CMIP5 archive, as suggested by Sonali et al. (2017), were selected and 4 among the selected climate models are common for both T_{max} and T_{min} (see Table 2 for details).

Natural variability was estimated from the pre-industrial control runs, represented as the 'piControl' experiment in CMIP5. The 9 model control simulations analyzed here comprise a total of 6276 yr for T_{max} and 4590 yr for T_{min}. The number of years of 'piControl' simulation availability varies across different climate models. Hence, addition of all climate models' control simulations leads to different numbers of years for T_{max} and T_{min}. To assess the possible effect of external forcings (anthropogenic and natural), different climate model simulations of CMIP5 such as 'historical,' 'historicalNat,' 'historicalGHG,' 'historical_AA' and 'historical_LU' were considered. Information on different experiments is available in Table 1, and more details can be found in the CMIP5 archive (https://cmip.llnl.gov/cmip5/docs/Taylor_CMIP5_design.pdf) (Taylor et al. 2012). The historicalMisc experiment represents the individual effect of historical forcings. CCSM4 provides individual forcing simulations of both T_{max} and T_{min}. In order to understand the effect of individual forcing only, simulations under land use forcing (historical_LU) and anthropogenic aerosol forcings (historical_AA) of CCSM4 climate model were considered for our attribution analysis. In historicalMisc experiments of the CCSM4 model, the r[1,4,6]i1p10 and r[1,4,6]i1p13 realizations respectively represent anthropogenic aerosol forcing (historical_AA) and land-use-change forcing (historical_LU) simulations.

All CMIP5 climate models provide 'historical' and 'piControl' simulations. The availability of different experiments (Table 2) was one of the criteria for selection of the climate models. To increase the robustness of this analysis and reduce the uncertainty, we used simulations from multiple climate models instead of just 1 set.

Ensemble means were first calculated for individual models over available realizations for each experiment separately. Averaging over multiple realizations for a particular climate model reduces the noise. The multi-model mean (MMM) was obtained for each experiment by taking the arithmetic average of the model-specific ensemble means. In this way equal weights are assigned to all models while calculating MMM. All considered GCMs have different spatial resolutions and are coarser than CRU data, i.e. 0.5° × 0.5°. Due to different spatial resolutions, all GCMs and CRU datasets were interpolated to a common grid of 1.5° latitude × 1.5° longitude by applying the inverse distance weighted (IDW) technique, which is one of the most widely used deterministic and robust approaches for spatial interpolation.

Table 1. Details of the CMIP5 experiments used in this study. Source: CMIP5 Coupled Model Intercomparison Project (https://cmip.llnl.gov/cmip5/data_portal.html)

Experiment	Description
piControl	Represents natural internal variability with fixed preindustrial greenhouse gases (GHGs) and no change in natural external factors such as solar irradiance and volcanic activities
historical	Forced by observed atmospheric composition of the 20th century; reflects both anthropogenic (well mixed GHGs, aerosols and ozone) and natural sources (solar and volcanic eruption)
historicalGHG	Driven by GHG forcing alone
historicalNat	Contains changes in solar irradiance and volcanic activity only
historical_AA	Simulations with anthropogenic aerosols (AA) forcing only
historical_LU	Simulations with land-use (LU) change forcing only

Temperature is one of the most important parameters with which to detect climate fluctuations because of its impact on different components of the hydrological cycle, such as streamflow, evapotranspiration and soil moisture. Both T_{max} and T_{min} are used as indicators for warming or cooling. The considered hydroclimatological datasets (i.e. T_{max} and T_{min}) of 3 temperature-homogenous regions were used for trend analysis. Trend analysis was carried out considering a gridwise dataset as well as a regionally averaged dataset over the 3 temperature-homogenous regions separately to assess the spatio-temporal behavior of climate over South India. Division of the seasons was based on conventional meteorological seasons: winter (January–February; JF), pre-monsoon (March–May; MAM), monsoon (June–September, JJAS) and post-monsoon (October–December; OND).

3. METHODS

The main steps involved in any formal detection and attribution study include the observation of one of the

Table 2. Details of the models used for maximum and minimum temperature (T_{max} and T_{min}) and the availability of different experiments (see Table 1) in these models. –: not available

No.	Model_T_{max}	Institution	piControl ≥500 yr	historical	historical Nat	historical_AA & historical_LU	historical GHG
1	CCSM4	National Center for Atmospheric Research	Yes	Yes	Yes	Yes	Yes
2	MIROC5	Atmosphere and Ocean Research Institute, National Institute for Environmental Studies, and Japan Agency for Marine-Earth Science and Technology	Yes	Yes	–	–	–
3	CESM1-BGC	National Science Foundation, Department of Energy, National Center for Atmospheric Research	Yes	Yes	–	–	–
4	CESM1-CAM5	National Science Foundation, Department of Energy, National Center for Atmospheric Research	No	Yes	–	–	–
5	CESM1_FASTCHEM	National Science Foundation, Department of Energy, National Center for Atmospheric Research	No	Yes	–	–	–
6	BNU-ESM	College of Global Change and Earth System Science, Beijing Normal University	Yes	Yes	Yes	–	Yes
7	CNRM-CM5	Centre National de Recherches Météorologiques	Yes	Yes	Yes	–	Yes
8	MPI-ESM LR	Max Planck Institute for Meteorology (MPI-M)–	Yes	Yes	–	–	–
9	MPI-ESM P	Max Planck Institute for Meteorology (MPI-M)	Yes	Yes	–	–	–

No.	Model_T_{min}	Institution	piControl ≥500 yr	historical	historical Nat	historical Misc	historical GHG
1	CCSM4	National Center for Atmospheric Research	Yes	Yes	Yes	Yes	Yes
2	MIROC5	Atmosphere and Ocean Research Institute, National Institute for Environmental Studies, and Japan Agency for Marine-Earth Science and Technology	Yes	Yes	–	–	–
3	CESM1-BGC	National Science Foundation, Department of Energy, National Center for Atmospheric Research	Yes	Yes	–	–	–
4	CESM1-CAM5	National Science Foundation, Department of Energy, National Center for Atmospheric Research	No	Yes	–	–	–
5	MRI-CGCM3	Meteorological Research Institute	Yes	Yes	Yes	–	Yes
6	NOR-ESM1 M	Norwegian Climate Centre	Yes	Yes	Yes	–	Yes
7	MIROC4h	Atmosphere and Ocean Research Institute, National Institute for Environmental Studies, and Japan Agency for Marine-Earth Science and Technology	No	Yes	–	–	–
8	GFDL-ESM2G	Geophysical Fluid Dynamics Laboratory	Yes	Yes	–	–	–
9	ACCESS1.3	CSIRO (Commonwealth Scientific and Industrial Research Organisation, Australia), and BOM (Bureau of Meteorology, Australia)	Yes	Yes	–	–	Yes

climate variables, an estimation of how the external drivers of climate have evolved before and during the considered time period, and a physical-based assessment of how the external drivers would have affected the observed climate variable. It is necessary to check whether the climatic trends are significant in the observation period prior to formal detection and attribution analysis. Statistical significances of trends present in seasonal and annual T_{max} and T_{min} series for the period 1950–2012 were quantified by applying a modified Mann-Kendall (MMK) approach and magnitude of trend using Sen's slope approach. Details about the MMK approach and Sen's approaches are provided in Appendices 1 & 2.

The detection phase checks whether the observed changes can be fully explained by the background 'noise' estimated from the piControl experiment. The attribution phase examines whether the observed changes are consistent with the 20th century climate simulation obtained from historical experiments and simultaneously inconsistent with the natural external climate simulation obtained from the historicalNat experiment. All climate model experiments used for the attribution analysis have data normally up to 2005 in the CMIP5 archive. Hence the formal detection and attribution study was conducted over a 56 yr period (1950–2005).

Fingerprint detection and attribution helps in assessing the extent to which patterns of response to external anthro-forcing from climate model simulations (i.e. fingerprints) explain observed climate change. This approach reduces the detection problem to a low dimensional space where human-induced climate change can be extracted smoothly from the noise, i.e. natural climate variability. The fingerprint specifies the direction of the signal induced by anthropogenic effects. This process is distinct from the extreme ways of detecting changes either in a full variable space or using means as representatives (Jia et al. 2012). An optimization process was used in previous studies (Santer et al. 2007, Hidalgo et al. 2009) to enhance the detectability of the fingerprint, but this requires a part of the piControl model simulation which cannot be used again for detection. Hidalgo et al. (2009) found a slight difference in results by employing optimized and non-optimized versions of the fingerprint approach. Hence here we used the non-optimized fingerprint approach, and the entire length of the control simulation was used for the detection process. The fingerprint, which explains the maximum variability, is specified as the leading empirical orthogonal function (EOF) of ensemble-averaged anthropogenically forced temperature time series (obtained from the historical experiment) of different considered climate models. The signal strength is calculated as the least squares linear trend of the projection of a data set (observations or model simulated) onto the fingerprint. So given the fingerprint $F(x)$, the signal strength S is determined as

$$S = trend[F(x) \cdot T(x,t)] \quad (1)$$

where $T(x,t)$ is the time series from observation or model simulation, and '*trend*' indicates the slope of the least squares best-fit line. Signal strength for observations and for various model simulations were obtained using the above equation. Significant changes observed in T_{max} and T_{min} could be attributed to different factors by comparing the signal strengths determined from different experiments with that of the observations. The fingerprint was estimated here by pooling the information from all models (considering the MMM). MMM ensemble average simulation performs better than individual climate model simulations because of the reduction in noise (Santer et al. 2007, Bonfils et al. 2008, Mondal & Mujumdar 2012). Uncertainty in signal strength was calculated from a Monte Carlo simulation. Data over each grid are expressed in anomaly form considering the climatological mean calculated over the entire period.

The detection process evaluates whether the observed significant changes have occurred due to natural variations in the climate system. Climate model simulations obtained from control integrations (piControl experiment) which include only natural internal variability (no forcing) of the climate system were considered for this process. A Monte Carlo test was used to estimate the likelihood that the observations are pulled from the control simulation obtained from the piControl experiment. The detection process was carried out for individual climate models which have at least 500 yr (as mentioned in Table 2) of control simulations as well as for the combined control simulations obtained from all climate models together. A step-by step procedure for fingerprint-based formal detection and attribution analysis is presented in Appendix 3.

4. RESULTS AND DISCUSSION

4.1. Analysis of temporal trends in T_{max} and T_{min}

Major changes in a time series can occur gradually (trends), abruptly (step-changes) or in a complex fashion, but long-term change specifies the impact of

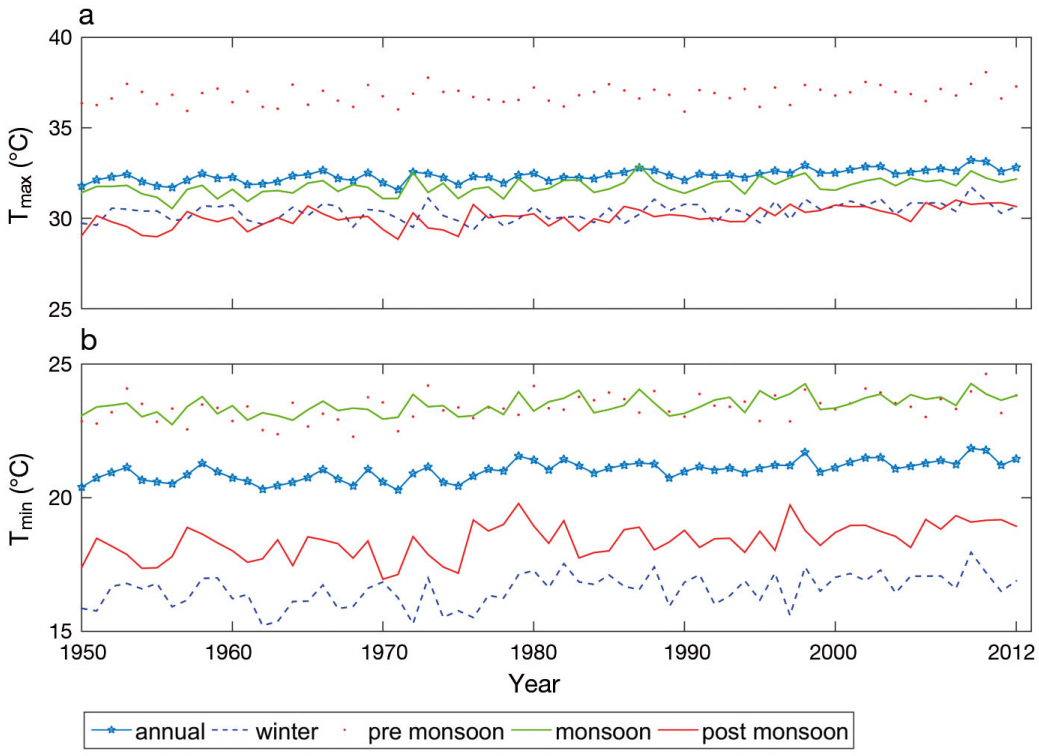

Fig. 2. Seasonal variation in (a) maximum temperature (T_{max}) and (b) minimum temperature (T_{min}) (°C) over South India for the period 1950–2012

climate change, the main focus of the present study. The widely used MMK approach which satisfies the independence assumption, explained in Appendix 1, was employed for trend analysis. On the basis of the observed time series (1950–2012) of seasonal and annual T_{max} and T_{min}, a detailed trend analysis was carried out and results are presented in Fig. 2 and Table 3.

Fig. 2 shows the variations of T_{max} and T_{min} in different seasons and annually over all of South India during 1950–2012. High values of T_{max} and T_{min} are seen during the pre-monsoon season, but T_{min} is also high during the monsoon season. T_{max} is lower during winter and post-monsoon seasons. T_{min} is lower during winter compared to other seasons. Analysis was also carried out for seasonal and annual T_{max} and T_{min} averaged over all of India and 3 temperature homogenous regions (EC, WC, IP) separately along with South India. Results for all regions are presented in Table 3. In Table 3, the symbol 'π', indicating time series, depicts an increasing trend at the 5% significance level. Significant upward trends appear in annual and seasonal T_{max} and T_{min} in South India (which includes EC, WC and IP regions). When considering individual regions (i.e. EC, WC, IP), similar conclusions (i.e. warming trend in all cases) were obtained. However, no trends are obvious in T_{min} over all of India during winter and pre-monsoon seasons. These significant changes may be due to rapid increases in urbanization and industrialization in recent decades. Using Sen's slope approach (Appendix 2), we found that the trend magni-

Table 3. Presence of trend using the modified Mann-Kendall approach. 'π' indicates the presence of a significant upward trend at the 5% significance level. Results are shown for all of India, South India and 3 temperature-homogenous regions (EC: east coast, WC: west coast, IP: interior peninsula) in different seasons during 1950–2012 for maximum and minimum temperature (T_{max} and T_{min})

	Detection variable	Annual	Winter	Pre-monsoon	Mon-soon	Post-monsoon
All of India	T_{max}	π	π	π	π	π
	T_{min}	π			π	π
South India	T_{max}	π	π	π	π	π
	T_{min}	π	π	π	π	π
EC	T_{max}	π	π	π	π	π
	T_{min}	π	π	π	π	π
WC	T_{max}	π	π	π	π	π
	T_{min}	π	π	π	π	π
IP	T_{max}	π	π	π	π	π
	T_{min}	π	π	π	π	π

tude is the same for both T_{max} and T_{min} over South India, highest during post-monsoon season around 0.02°C yr^{-1}. Warming in seasonal T_{min} is more acute in all seasons compared to T_{max} except in the post-monsoon season. These results indicate a significant change in climate.

Furthermore, gridwise trends of T_{max} and T_{min} over South India were obtained for different seasons for the period 1950–2012. As discussed in Section 2.1, 428 grid points of the CRU3.22 dataset cover all of South India (shown in Fig. 1). Large numbers of grid points covering South India exhibit significant change. Significant changes are computed as the percentage change over the time period in seasonal T_{max} and T_{min} using the MMK approach. Changes over the period during different seasons in T_{max} are 50% (winter), 50% (pre-monsoon) and 41% (monsoon) and in T_{min} are 55% (winter), 70% (pre-monsoon) and 78% (post-monsoon). Results are shown in Fig. 3 only for the seasons when T_{max} and T_{min} have highest significant trends. More than 93% of the total grid points witnessed significant upward trends in T_{min} during the monsoon season. Similarly, 82% of the grid points for T_{max} show significant upward trends during the post-monsoon season (Fig. 3). Overall change in percentage is higher in T_{min} compared to T_{max}.

Cloudiness is strongly associated with both T_{max} and T_{min}. T_{max} decreases as cloudiness increases and vice versa, but the net effect on T_{min} is less. T_{min} goes down with an increase in cloudiness, whereas downward longwave radiation tends to increase and leads to increases in T_{min}. To summarize, an increase in cloudiness is the reason for change (decrease) in the diurnal temperature range (Rai et al. 2012). Jaswal (2017) analyzed seasonal variability and changes in cloud cover during the period 1951–2010 utilizing datasets of 195 surface meteorological stations covering all of India provided by IMD. Results indicated an overall significant decrease in the mean total cloud cover in most parts of India during all 4 seasons (winter, pre-monsoon, monsoon and post-monsoon) except in the Indo-Gangetic plains and the northeast region (where cloud cover has increased). Analysis on spatial distribution of cloud cover climatology showed high magnitude over the southern peninsula, Western Ghats and the northeast region of India. The study by Jaswal (2017) is highly relevant for the present analysis as it is considered a substitute for cloud cover analysis for our study in the absence of a freely available cloud cover dataset from IMD. Moreover, the time period considered by Jaswal (2017) is nearly the same as in our analysis, and our present study area, i.e. South India, is also a part of their analysis. Decreasing trends in cloud cover in many parts of India, including the southern part (our study area), is of interest especially given significant observed changes in T_{max} and T_{min}. Regional analysis by Warren et al. (2007) also indicated significant decreasing trends of total cloud cover in India. Diminishing trends of annual total cloud cover were observed during 1952–1997 in the Krishna basin of South India (Biggs et al. 2007). Revadekar et al. (2013) found that the changes in temperature extremes at low altitude over

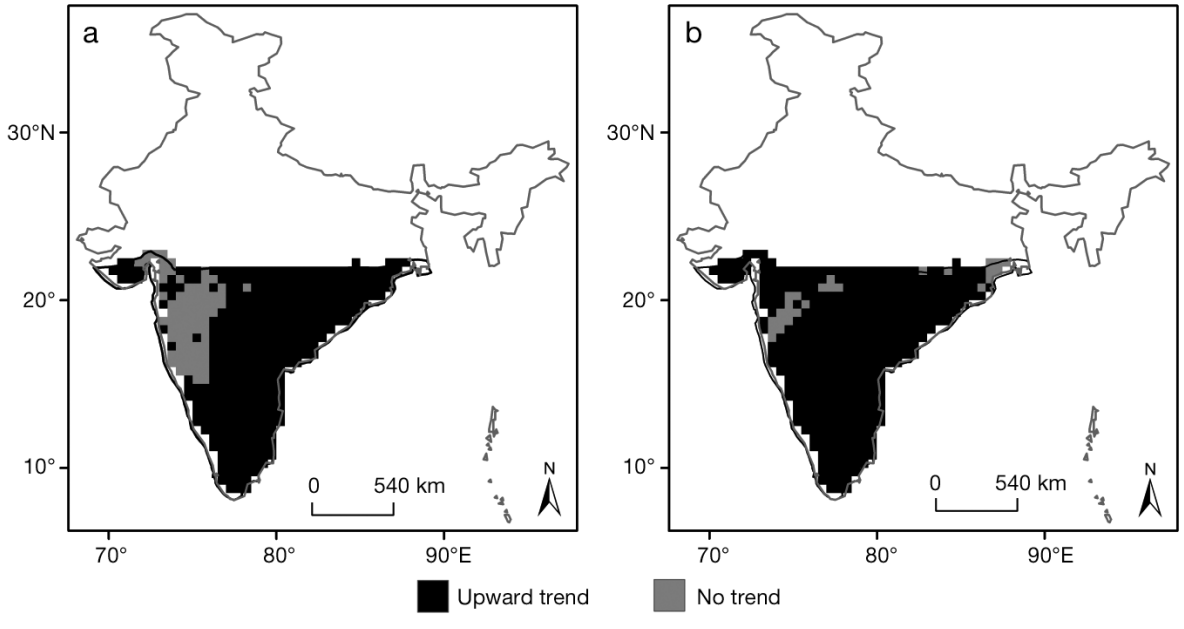

Fig. 3. Trends in (a) post-monsoon maximum temperature (T_{max}) and (b) monsoon minimum temperature (T_{min})

South Asia are less sensitive to local and regional factors compared to high altitude. These studies could partially explain the reason for the significant temperature changes in South India. Urbanization has a large impact on regional climatic trends and usually induces warming. Hence the impact of urbanization on the temperature trend is crucial and mainly affects T_{min} compared to T_{max}. A limitation of the present study could be excluding urbanization effect on climate change because of lack of qualitative datasets (of at least 50 yr). However, fingerprint-based formal detection and attribution analysis (presented below) adopted CMIP5 model simulations from different experiments which broadly consider the effect of the above factors (simulations under land use forcing i.e. historical_LU).

Relative humidity (RH) is the measurement of actual moisture content of the atmosphere expressed as the percentage of the maximum possible moisture content. The water holding capacity of the atmosphere depends on the temperature of the surrounding atmosphere. Over land areas (under limiting moisture conditions), RH decreases with increasing temperature, suggesting dryness/wetness at high/low temperatures, respectively. RH has an important implication for climate impact assessment studies. Hence, we analyzed RH trends in conjunction with temperature. A dataset of observed RH covering the period 1950–2012 was not available. Therefore, a monthly mean surface RH dataset at 2.5° × 2.5° resolution (global in coverage) sourced from the National Center for Environmental Prediction was derived. Trend analysis was performed at seasonal and annual time scales employing the MMK approach. Results indicate that RH exhibited significant decreasing trends over South India during all seasons except winter. Trends were significant in annual, pre-monsoon and monsoon RH at 5% and post-monsoon RH at 10% significance level. This downward trend in RH may be due to the significant warming observed in South India over the same time frame. These results can be considered as evidence of the observed warming induced because of anthropogenic influence. To date, no study in India has validated the RH in climate models, largely because of the unavailability of suitable datasets. In the future, such validation of RH deserves increased attention, as RH is one of the vital thermal parameters which can be employed for climate change detection and attribution studies.

It is clear from the trend analysis (using MMK) that South India experienced significant temperature changes during 1950–2012. Changes in seasonal climate patterns in South India and their connection to large-scale circulations are important to understand. Sea surface temperature (SST) plays a significant role in shaping climate and helps in understanding seasonal climatic patterns and extreme heat and cold events. Both Indian Ocean and Pacific Ocean SSTs play a crucial role in modulating Indian climate, and this is strongly supported by previous studies (Gadgil 2003). The influence of large-scale circulation on the climate of South India was analyzed by considering different climatic indices at a seasonal scale. The El Niño Southern Oscillation (ENSO) and Indian Ocean Dipole (IOD) are the principal drivers of internal climate variability in the Pacific and Indian Oceans, respectively. The Niño3.4 index and dipole mode index (DMI), estimated based on SST, are oceanic components of ENSO and IOD. Similarly, the atmospheric components of ENSO and IOD, such as the Southern Oscillation index (SOI) (based on sea level pressure differences between Tahiti and Darwin) and Equatorial zonal wind index (EQWIN) (based on surface zonal wind averaged over the central equatorial Indian Ocean) (Francis & Gadgil 2013), were adopted here. EQWIN is the index used for the Equatorial Indian Ocean Oscillation (EQUINOO), which is the atmospheric component of the IOD. El Niño and La Niña, part of ENSO, are among the most powerful climatic phenomena on Earth, cycles of warm and cold temperature episodes over the globe in accordance with the changing patterns of SST over the Pacific. SOI represents the strength of El Niño and La Niña events. Seasonal time series of T_{max} and T_{min} averaged over South India are linked with the respective climatic indices. To demonstrate the lead–lag relationship, lag (by 1 and 2 seasons), concurrent and lead (by 1 and 2 seasons) correlations of large-scale circulation indices with T_{max} and T_{min} at a seasonal scale were obtained, and the results are presented in Table 4. The association of ENSO is stronger as compared to IOD. The correlation of T_{max} and T_{min} with the Niño3.4 index is high and positive. Hence, in Table 4, the number of significant correlations is higher in the case of Niño3.4 compared to other indices, which is the usual notion (Francis & Gadgil 2013, Pattanayak et al. 2017). Hence, it can be concluded that the seasonal temperature patterns of South India are strongly linked to the ENSO. In contrast, IOD is poorly correlated with both T_{max} and T_{min} during the same time frame.

ENSO is an important global climatic phenomenon. It could be driven by both natural and anthropogenic changes in the climate. Naturally occurring ENSO events (El Niño and La Niña) and human-

Table 4. Lead–lag and simultaneous correlation between the climatic indices (Niño3.4, SOI, DMI, EQWIN; see section 4.1 for details) and maximum and minimum temperature (T_{max}, T_{min}) of South India during different seasons for the time period 1950–2012. + and – respectively indicate a significant positive and negative correlation at the 5% level

Index		Winter					Pre-monsoon					Monsoon					Post-monsoon				
		Lag			Lead		Lag			Lead		Lag			Lead		Lag			Lead	
		2	1	0	1	2	2	1	0	1	2	2	1	0	1	2	2	1	0	1	2
Niño3.4	T_{max}	+	+	+	+		+	+				+	+	+	+	+		+	+	+	+
	T_{min}	+	+	+	+		+	+	+			+	+	+	+		+	+	+	+	+
SOI	T_{max}	–											–	–	–			–			
	T_{min}	–	–	–			–	–					–		–			–	–	–	–
DMI	T_{max}					–															
	T_{min}																		+		
EQWIN	T_{max}								–		–										
	T_{min}				–	–			–	–	–										

induced climate change are closely associated, and naturally occurring ENSO events are going to be heightened in conjunction with global warming (Stocker et al. 2013).

4.2. Formal detection and attribution analysis

Unlike trend analysis (temporal variation), fingerprint-based detection and attribution analysis provides spatio-temporal information. The 'fingerprints' are usually derived from changes simulated by a climate model in response to anthropogenic forcing. Detection variables used for this analysis include seasonal and annual averaged T_{max} and T_{min} linked directly to hydrological changes. Formal detection and attribution was performed in a multi-model frame work. Models of CMIP5 produce historical simulations until 2005, hence formal detection and attribution analysis was based on the period 1950–2005. Fingerprints are the leading EOFs of the seasonal T_{max} and T_{min} time series during 1950–2005. For all detection variables, i.e. annual T_{max}, JF T_{max}, MAM T_{max}, JJAS T_{max}, OND T_{max}, annual T_{min}, JF T_{min}, MAM T_{min}, JJAS T_{min} and OND T_{min}, fingerprints were calculated separately using the MMM historical simulation. Historical simulations of the ACCESS1.3 model for T_{min} differed significantly from the MMM historical simulation (based on a nonparametric Wilcoxon signed rank test). This behaviour is seen only during the pre-monsoon season, so the ACCESS1.3 climate model was excluded from fingerprint estimation of pre-monsoon T_{min} (MAM T_{min}).

Before conducting attribution analysis, a Monte Carlo test (as explained in Appendix 3) was used to estimate the likelihood of the observed signal strengths being extracted from piControl signal strength distributions. Control signal strengths were calculated in segments of 56 yr to match the observed record. By combining control simulations from all models (9 each for T_{max} and T_{min}), we obtained and used a total of 6276 yr of T_{max} and 4590 yr of T_{min} data for this test. Models having at least 500 yr of data were considered separately for the Monte Carlo test. Seven out of 9 models satisfied this criterion for both T_{max} and T_{min} (Table 2). For observations, the number of sources (p) was considered as 1. Fifty-six years of non-overlapping p members were selected randomly from the total control simulations to obtain control signal strength. By iterating the process 10 000 times, the distribution of control signal strength was established and used to compare with the observed signal strength. This test was repeated for 7 models (piControl simulation ≥500 yr) individually and for a combination of all models. Here we presumed that if the observed signal strength falls outside the range of control simulations most of the time (including the combination of all models), then the observed changes are statistically different from natural climate variability. Results of this test shown in Table 5 indicate that change in 3 out of 10 detection variables, i.e. OND T_{max}, MAM T_{min} and JJAS T_{min} are statistically different from natural variability at the 5% significance level. Despite qualitative similarity in the detection result, uncertainty still exists and is model sensitive. In the case of the 3 detected variables, significance was not achieved in all cases (i.e. for all models or combination of models as shown in Table 5). For example, the observed signal strength for OND T_{max} was not statistically different from the control signal strength when CNRM_CM5 and MIROC5 models were considered. Hence, it is important to estimate signal strength (i.e. control simulations) from multiple climate models. The Monte Carlo test was repeated to check whether

Table 5. Results from the comparison study to determine whether the observed signal strengths are different from the control signal strength. ns and * respectively indicate statistically not different and different at the 5% significance level

Climate model (T_{max}) 'piControl' experiment	Annual T_{max}	JF T_{max}	MAM T_{max}	JJAS T_{max}	OND T_{max}
Combined (all models) (T_{max})	ns	ns	ns	ns	*
CCSM4	ns	ns	ns	ns	*
MIROC5	ns	ns	ns	ns	ns
CESM1_BGC	ns	ns	ns	ns	*
BNU_ESM	ns	ns	ns	ns	*
CNRM_CM5	ns	ns	ns	ns	ns
MPI_ESM_LR	ns	ns	ns	ns	*
MPI_ESM_P	ns	ns	ns	ns	*
Climate model (T_{min}) 'piControl' experiment	Annual T_{min}	JF T_{min}	MAM T_{min}	JJAS T_{min}	OND T_{min}
Combined (all models) (T_{min})	ns	ns	*	*	ns
CCSM4	ns	ns	*	*	ns
MIROC5	*	*	*	*	*
ACCESS1_3	ns	ns	*	*	ns
CESM1_BGC	ns	ns	ns	*	ns
GFDL_ESM2G	ns	ns	*	*	ns
MRI_CGCM3	ns	ns	*	*	ns
NORESM1_M	ns	ns	*	*	ns

the anthropogenic signal strengths obtained from the historical experiment are statistically different from the control signal strengths. In all cases, anthropogenic signal strengths differed significantly from the distribution of control signal strength.

Once detection was confirmed, analysis was further conducted to attribute those changes to several possible explanations obtained from historical, historicalNat, historicalGHG, historical_LU and historical_AA experiments. Signal strengths and corresponding 95% confidence intervals were obtained for model simulations under different experiments along with observations using Eq. (1). Observed signal strengths were compared with the individual and MMM model signal strengths of different experiments to attribute the observed detected changes to different inducive factors. Results for the individual cases of OND T_{max}, MAM T_{min} and JJAS T_{min} are shown in Figs. 4–6, respectively.

The observed signal strengths were consistent with the multi-model mean signal strengths of the historical experiment (Figs. 4–6). In all 3 detected variables, i.e. OND T_{max}, MAM T_{min} and JJAS T_{min}, values of MMM signal strength of the historical experiment were the same as the observed signal strength (~0.1). Note that here the fingerprint has negative loadings so the sign of signal strengths are inverted. However, signal strengths of the historicalNat experiment are mostly close to 0 and possess the opposite sign of the observed signal

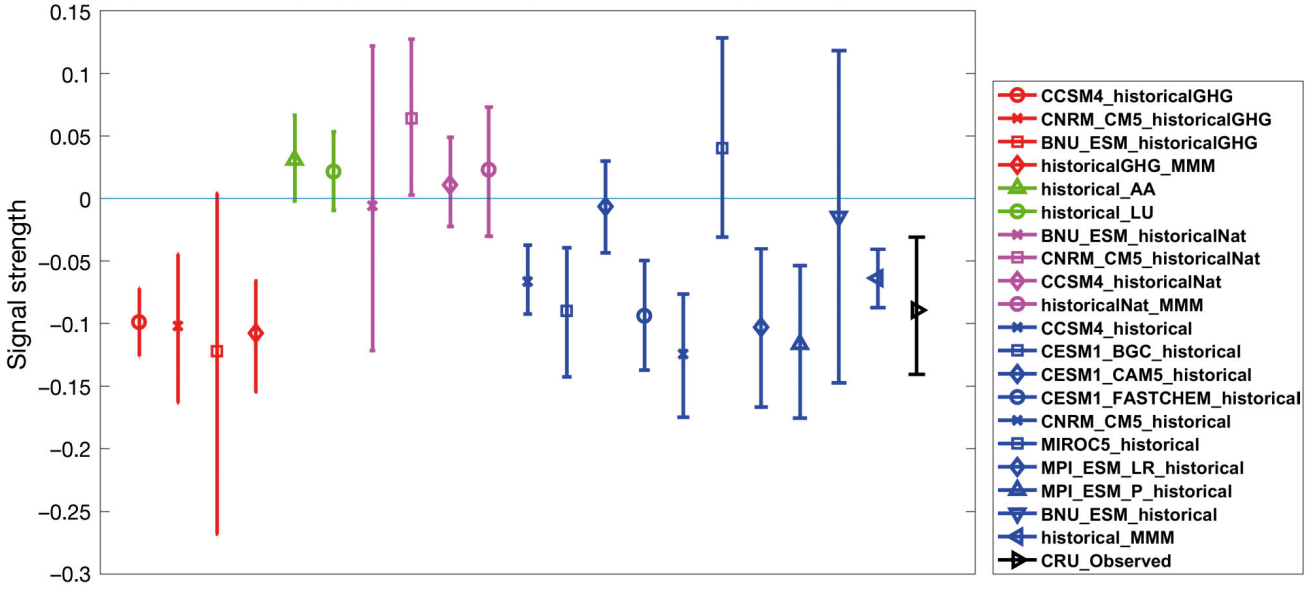

Fig. 4. Signal strengths and their 95% confidence intervals for various model experiments (individual and multi-model mean, MMM) and observation for post-monsoon maximum temperature (OND T_{max}). Signal strengths are shown consecutively for historicalGHG (red), historical_LU (green), historical_AA (green), historicalNat (pink) and historical (blue) experiments (see Table 1) for individual models and then MMM. Observed signal strength is shown in black

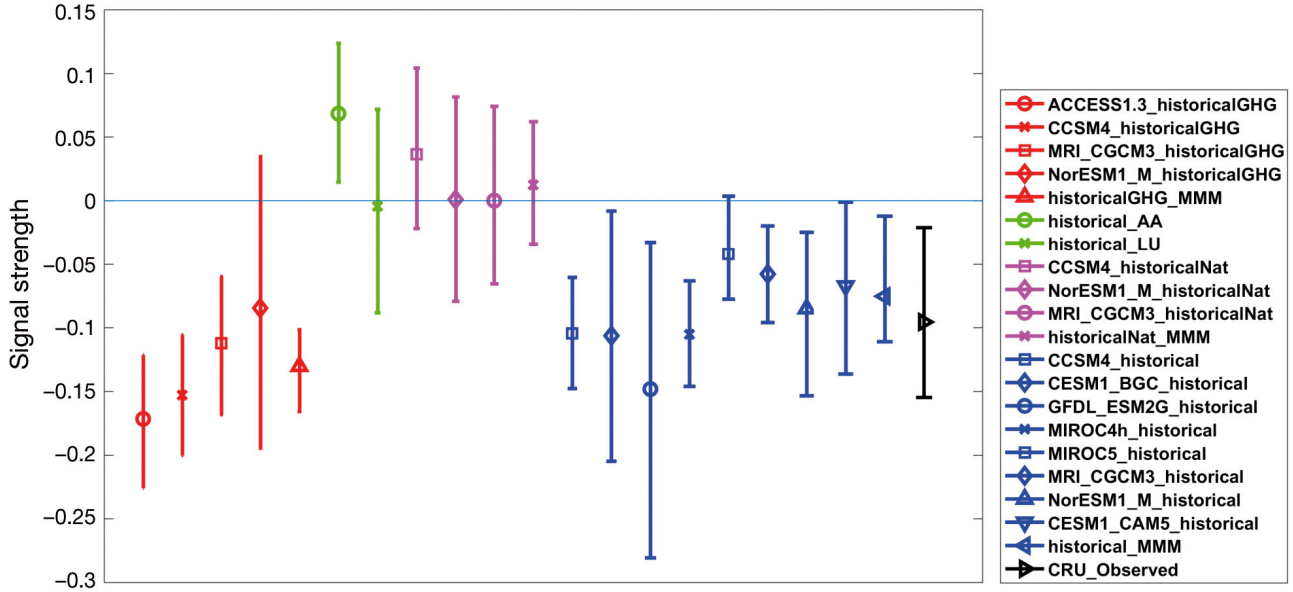

Fig. 5. As in Fig. 4, for pre-monsoon minimum temperature (MAM T_{min})

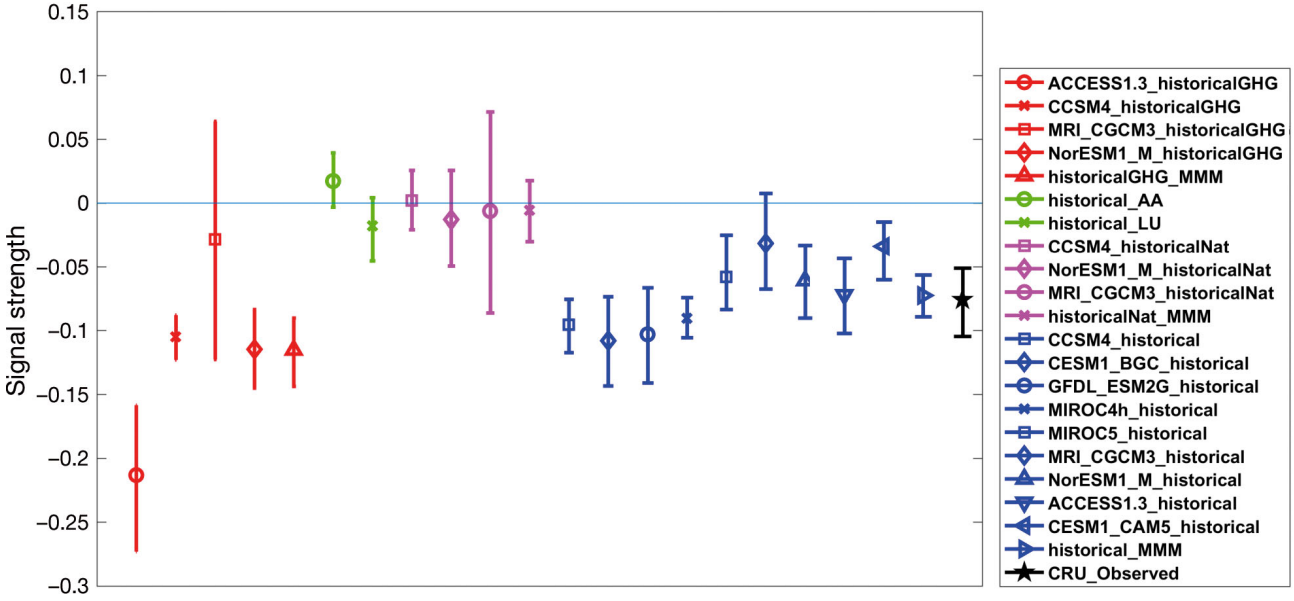

Fig. 6. As in Fig. 4, for monsoon minimum temperature (JJAS T_{min})

strengths. This implies that the combined effect of anthropogenic and natural forcings, represented by the historical experiment, could explain the recently observed changes in temperature over South India, whereas natural external forcings such as solar variability and volcanic activity could not. Observed changes in temperature can only be attributed to human-induced climate change.

Signal strength of observation and MMM signal strength obtained from the historicalGHG experiment (values are slightly >0.1 for all 3 detected variables) are very close and their difference is statistically small. However, the effects of anthropogenic aerosols and land-use forcing, which is represented by the signal strengths of the historical_AA and historical_LU experiments (green in Figs. 4–6), are not consistent with observed temperature changes over South India (impact of anthropogenic aerosols and land-use forcing are indistinct, as the signal strength magnitudes are low). The effects of GHGs (i.e. historicalGHG) can be attributed in the observed temperature changes in South India (as shown in Figs. 4–6). The effect of GHG forcing is dominant and clearly distinguishable compared to other external forcings (such as LU and AA).

This study was able to formally establish the footprint of anthropogenic climate change over South India. Human influences on climate are evident from natural internal or external variability. Findings of this fingerprint-based formal detection and attribution analysis are relevant in terms of assessing changes in climate and implementing these changes for future planning and adaption. Scope for uncertainties may arise as a result of considering the mean of multiple models by fixing equal weights for each of them (Knutti et al. 2010), detection methodology and ignorance of regional land use change information. To an extent, uncertainties can be reduced by considering shortlisted climate models from a prior evaluation study, instead of choosing arbitrarily (Sonali et al. 2017). Another avenue for further climate change detection and attribution analysis is by implementing different approaches considering various hydroclimatic variables. These aforementioned issues will be considered as major focal areas of future work.

5. CONCLUSION

The southern part of India is highly sensitive to climate change effects because of its varied climate and geography. Rapid changes and vulnerability in hydro-climatology during recent decades motivated us to further analyze the cause of observed changes over South India. Therefore, the goal of this investigation was to comprehensively analyze the changes in the South Indian climate, focusing primarily on T_{max} and T_{min}, initially by conducting trend analysis and then extensively by implementing fingerprint-based formal detection and attribution analysis. The fingerprint-based detection and attribution approach necessitates assessing the level of correspondence between model-simulated patterns of externally forced changes and observed changes for the considered time period.

To evaluate changes in South Indian climate, temporal variations in seasonal and annual T_{max} and T_{min} were analyzed for the period 1950–2012. The MMK approach was applied to cope with the autocorrelation of the time series. A pervasive increase in T_{max} and T_{min} is evidenced consistently during all seasons. Moreover, gridwise analysis revealed that the spread of significant changes in T_{min} is larger compared to T_{max} over South India. Spatial extensions of significant changes (number of grid points with significant trends) are higher in monsoon and post-monsoon seasons compared to other seasons respectively for T_{min} and T_{max}. The identified downward RH trends in most seasons could be due to the observed warming induced by anthropogenic influences. The impact of ENSO and IOD on Indian climate was found to be dominant. Hence the associations of South Indian T_{max} and T_{min} with ENSO and IOD were examined. ENSO had a stronger influence compared to IOD on seasonal temperature change patterns. We observed that the Niño3.4 index was associated significantly with seasonal T_{min} and T_{max} compared to other climatic indices.

Formal detection and attribution analysis revealed that the changes ascertained in T_{max} during the post-monsoon and T_{min} during the pre-monsoon and monsoon seasons in South India during 1950–2005 were detectably different from natural variability. Simultaneously, model-simulated natural external variability (specifying solar and volcanic effect) did not explain the observed changes. Changes in the observed temperature in South India can be attributed confidently to climate change induced by anthropogenic effects. Land use change alone cannot explain the observed changes in temperature, but the effect of GHGs is clearly detected in the temperature changes and is one of the major contributing factors.

Overall, South India is more susceptible to temperature changes, and more importantly, these changes are no longer natural. These findings presage grave consequences for processes such as hydrology, climatology, ecology, environmental engineering and forestry both at global and local scales.

Acknowledgements. This research was supported by the Divecha Centre for Climate Change, Indian Institute of Science. We acknowledge the World Climate Research Programme's Working Group on Coupled Modeling, which is responsible for CMIP, and thank all of the climate modeling groups for producing and making available their model outputs. For CMIP, the US Department of Energy's Program for Climate Model Diagnosis and Intercomparison provided coordinating support and led to the development of software infrastructure in partnership with the Global Organization for Earth System Science Portals. We also thank the IMD for the gridded temperature dataset.

LITERATURE CITED

Biggs TW, Scott CA, Rajagopalan B, Turral HN (2007) Trends in solar radiation due to clouds and aerosols, southern India. 1952–1997. Int J Climatol 27:1505–1518

Bindoff NL, Stott PA, Achuta Rao KM, Allen MR and others (2013) Detection and attribution of climate change: from global to regional. In: Stocker TF, Qin D, Plattner GK, Tignor M and others (eds) Climate change 2013: the physical science basis. Contribution of Working Group I

to the Fifth Assessment Report of the Intergovernmental Panel on Climate Change. Cambridge University Press, Cambridge, p 867–952

Bonfils C, Santer BD, Pierce DW, Hidalgo HG and others (2008) Detection and attribution of temperature changes in the mountainous western United States. J Clim 21: 6404–6424

Carleton TA (2017) Crop-damaging temperatures increase suicide rates in India. Proc Natl Acad Sci 114:8746–8751

Chithra NR, Thampi SG (2015) Detection and attribution of climate change signals in precipitation in the Chaliyar River basin, Kerala, India. Aquat Procedia 4:755–763

Cho C, Li R, Wang SY, Yoon JH, Gillies RR (2016) Anthropogenic footprint of climate change in the June 2013 northern India flood. Clim Dyn 46:797–805

Easterling DR, Horton B, Jones PD, Peterson TC and others (1997) Maximum and minimum temperature trends for the globe. Science 277:364–367

Francis PA, Gadgil S (2013) A note on new indices for the equatorial Indian Ocean oscillation. J Earth Syst Sci 122: 1005–1011

Gadgil S (2003) The Indian monsoon and its variability. Annu Rev Earth Planet Sci 31:429–467

Guhathakurta P, Sreejith OP, Menon PA (2011) Impact of climate change on extreme rainfall events and flood risk in India. J Earth Syst Sci 120:359–373

Harris I, Jones PD, Osborn TJ, Lister DH (2014) Updated high-resolution grids of monthly climatic observations-the CRU TS3.10 dataset. Int J Climatol 34:623–642

Hasselmann K (1993) Optimal fingerprints for the detection of time-dependent climate change. J Clim 6:1957–1971

Hidalgo HG, Das T, Dettinger MD, Cayan DR and others (2009) Detection and attribution of streamflow timing changes to climate change in the Western United States. J Clim 22:3838–3855

Jaswal AK (2017) Variability and changes in cloud cover over India during 1951–2010. In: Rajeevan MN, Nayak S (eds) Observed climate variability and change over the Indian region. Springer, Singapore, p 107–127

Jia Y, Ding X, Wang H, Zhou Z, Qiu Y, Niu C (2012) Attribution of water resources evolution in the highly water stressed Hai River Basin of China. Water Resour Res 48:W02513

Kendall MG (1975) Rank correlation methods. Charles Griffin, London

Khaliq MN, Ouarda TBMJ, Gachon P, Sushama L, St-Hilaire A (2009) Identification of hydrologic trends in the presence of serial and cross correlations. A review of selected methods and their application to annual flow regimes of Canadian rivers. J Hydrol (Amst) 368:117–130

Knutti R, Furrer R, Tebaldi C, Cermak J, Meehl GA (2010) Challenges in combining projections from multiple climate models. J Clim 23:2739–2758

Kothawale DR, Revadekar JV, Rupa Kumar K (2010) Recent trends in pre-monsoon daily temperature extremes over India. J Earth Syst Sci 119:51–65

Kumar N, Jaswal AK, Mohapatra M, Kore PA (2016) Spatial and temporal variation in daily temperature indices in summer and winter seasons over India (1969–2012). Theor Appl Climatol 129:1227–1239

Lau WKM and Kim KM (2010) Fingerprinting the impacts of aerosols on long term trends of the Indian summer monsoon regional rainfall. Geophys Res Lett 37:L16705

Mann HB (1945) Nonparametric tests against trend. Econometrica 13:245–259

Mishra V, Kumar D, Ganguly AR, Sanjay J, Mujumdar M, Krishnan R, Shah RD (2014) Reliability of regional and global climate models to simulate precipitation extremes over India. J Geophys Res Atmos 119:9301–9323

Mondal A, Mujumdar PP (2012) On the basin scale detection and attribution of human induced climate change in monsoon precipitation and streamflow. Water Resour Res 48:W10520

Mondal A, Mujumdar PP (2015) On the detection of human influence in extreme precipitation over India. J Hydrol 529:1161–1172

Pattanayak S, Nanjundiah RS, Kumar DN (2017) Linkage between global sea surface temperature and hydroclimatology of a major river basin of India before and after 1980. Environ Res Lett 12:124002

Rai A, Joshi MK, Pandey AC (2012) Variations in diurnal temperature range over India: under global warming scenario. J Geophys Res Atmos 117:D02114

Raju KS, Sonali P, Nagesh Kumar D (2016) Ranking of CMIP5 based global climate models for India using compromise programming. Theor Appl Climatol 128: 563–574

Revadekar JV, Hameed S, Collins D, Manton M and others (2013) Impact of altitude and latitude on changes in temperature extremes over South Asia during 1971–2000. Int J Climatol 33:199–209

Ribes A, Azaïs JM, Planton S (2009) Adaptation of the optimal fingerprint method for climate change detection using a well-conditioned covariance matrix estimate. Clim Dyn 33:707–722

Ribes A, Planton S, Terray L (2013) Application of regularized optimal fingerprinting to attribution. Part I: method, properties and idealized analysis. Clim Dyn 41: 2817–2836

Rupa Kumar K, Krishna Kumar K, Pant GB (1994) Diurnal asymmetry of surface temperature trends over India. Geophys Res Lett 21:677–680

Santer BD, Mears C, Wentz FJ, Taylor KE and others (2007) Identification of human-induced changes in atmospheric moisture content. Proc Natl Acad Sci USA 104:15248–15253

Sen PK (1968) Estimates of the regression coefficient based on Kendall's tau. J Am Stat Assoc 63:1379–1389

Singh R, Kumar R (2015) Vulnerability of water availability in India due to climate change: a bottom-up probabilistic Budyko analysis. Geophys Res Lett 42:9799–9807

Sonali P, Nagesh Kumar D (2013) Review of trend detection methods and their application to detect temperature changes in India. J Hydrol 476:212–227

Sonali P, Nagesh Kumar D (2016a) Detection and attribution of seasonal temperature changes in India with climate models in the CMIP5 archive. J Water Clim Change 7:83–102

Sonali P, Nagesh Kumar D (2016b) Spatio-temporal variability of temperature and potential evapotranspiration over India. J Water Clim Change 7:810–822

Sonali P, Nagesh Kumar D, Nanjundiah RS (2017) Intercomparison of CMIP5 and CMIP3 simulations of the 20th century maximum and minimum temperatures over India and detection of climatic trends. Theor Appl Climatol 128:465–489

Srivastava AK, Rajeevan M, Kshirsagar SR (2009) Development of a high resolution daily gridded temperature data set (1969–2005) for the Indian region. Atmos Sci Lett 10: 249–254

Stocker TF, Qin D, Plattner GK, Tignor M and others (eds) (2013) Climate change 2013: the physical science basis. Contribution of Working Group I to the 5th Assessment Report of the Intergovernmental Panel on Climate Change. Cambridge University Press, Cambridge

Stone DA, Hansen G (2016) Rapid systematic assessment of the detection and attribution of regional anthropogenic climate change. Clim Dyn 47:1399–1450

Taylor KE, Stouffer RJ, Meehl GA (2012) An overview of CMIP5 and the experiment design. Bull Am Meteorol Soc 93:485–498

Vinnarasi R, Dhanya CT, Chakravorty A, AghaKouchak A (2017) Unravelling diurnal asymmetry of surface temperature in different climate zones. Sci Rep 7:7350

Warren SG, Eastman RM, Hahn CJ (2007) A survey of changes in cloud cover and cloud types over land from surface observations. 1971–96. J Clim 20:717–738

Watanabe M, Suzuki T, O'ishi R, Komuro Y and others (2010) Improved climate simulation by MIROC5: mean states, variability, and climate sensitivity. J Clim 23: 6312–6335

Yue S, Wang CY (2004) The Mann-Kendall test modified by effective sample size to detect trend in serially correlated hydrological series. Water Resour Manag 18:201–218

Zhou L, Dickinson RE, Dai A, Dirmeyer P (2010) Detection and attribution of anthropogenic forcing to DTR changes from 1950 to 1999: comparing multi-model simulations with observations. Clim Dyn 35:1289–130766

Appendix 1. Modified Mann-Kendall (MMK) approach by variance correction

Slope-based parametric approaches such as linear regression need to fulfill both distributional and independence assumptions, whereas nonparametric approaches are independent of distributional assumptions. In the present study, none of the time series (seasonal and annual) followed a normal distribution as determined by a Kolmogorov-Smirnov test (KS-test). The nonparametric Mann-Kendall (MK) approach is particularly useful to identify the presence of significant trends in hydroclimatological series (Mann 1945, Kendall 1975). In the MK test, the null hypothesis is that 'no trend exists in the time series' and the alternate hypothesis is that 'a trend exists with a significance level' by assuming data to be independent.

The MK test statistic S_{MK} is computed as

$$S_{MK} = \sum_{i=1}^{n-1} \sum_{j=i+1}^{n} sign(T_j - T_i) \quad \text{(A1)}$$

where T_i and T_j are 2 sequential subseries of data and n is the length of the data series. T_i is used as a reference point of T_j employing the equations:

$$sign(T_j - T_i) = \begin{cases} -1 \text{ for } (T_j - T_i) < 0 \\ 0 \text{ for } (T_j - T_i) = 0 \\ 1 \text{ for } (T_j - T_i) > 0 \end{cases} \quad \text{(A2)}$$

$$\mathrm{E}[S_{MK}] = 0 \quad \text{(A3)}$$

$$Var(S_{MK}) = \frac{n(n-1)(2n+5) - \sum_{k-1}^{q} p_k(p_k-1)(2p_k+5)}{18} \quad \text{(A4)}$$

where p_k is the number of ties of extent for the k^{th} value and q is the number of tied groups. In the variance formula, the second part of the numerator is considered for tied censored data. The standard MK test statistic Z_{MK} is described by the following equation:

$$Z_{MK} = \begin{cases} \frac{S_{MK}-1}{\sqrt{Var(S_{MK})}} \text{ if } S_{MK} > 0 \\ 0 \text{ if } S_{MK} = 0 \\ \frac{S_{MK}+1}{\sqrt{Var(S_{MK})}} \text{ if } S_{MK} < 0 \end{cases} \quad \text{(A5)}$$

If $|Z_{MK}|$ is greater than $Z_{\alpha/2}$, where α represents the assumed significance level (5%), then the null hypothesis is rejected implying that the trend is significant. $Z_{\alpha/2}$ is obtained from the standard normal table.

In spite of the robustness of the MK test for the distributional aspect of data, it does not consider the effect of serial correlation. Improper independence assumption in a statistical test may lead to erroneous conclusions by heightening the chance of type-1 errors. Various studies (Khaliq et al. 2009, Sonali & Nagesh Kumar 2013) have strongly supported the consideration of effects of serial correlation in the usual trend detection practice. Hence, to limit the effect of serial correlation on the trend detection analysis, we used the modified MK (MMK) approach suggested by Yue & Wang (2004). The presence of serial correlation affects the variance of the MK test statistic. Hence a correction factor is used to obtain the modified variance:

$$Var^{\star}(S_{MK}) = Var(S_{MK}) \cdot \frac{n}{n^{\star}} \quad \text{(A6)}$$

The following equation is used to compute $n^{\star}$:

$$n^{\star} = \frac{n}{1 + 2 \cdot \sum_{k=1}^{n-1} (1 - \frac{k}{n})\ r_k} \quad \text{(A7)}$$

where $n^{\star}$ is the effective sample size which is uncorrelated out of total n of data points in a time series. r_k is the lag-k serial correlation coefficient and is computed as:

$$r_k = \frac{\frac{1}{n-k} \sum_{t=1}^{n-k} (X_t - \bar{X}_t)(X_{t+k} - \bar{X}_t)}{\frac{1}{n} \sum_{t=1}^{n} (X_t - \bar{X}_t)^2} \quad \text{(A8)}$$

$$\bar{X}_t = \frac{1}{n} \sum_{t=1}^{n} X_t \quad \text{(A9)}$$

Appendix 2. Sen's slope approach

Sen (1968) developed a non-parametric procedure to estimate the magnitude of a trend in the sample of n pairs of data. It is one of the most commonly used approaches to detect linear trends (Khaliq et al. 2009). The slope is estimated as follows:

$$Q_i = \left[\frac{(T_j - T_i)}{(j - i)}\right] \text{for all } i = 1, 2\ldots, n \quad \text{(B1)}$$

The n values of Q_i are kept in an ascending order to obtain the median value. Sen's slope Q_{sen} is computed as:

$$Q_{sen} = \begin{cases} Q_{(n+1)/2} & \text{if } n \text{ is odd} \\ \dfrac{Q_{n/2} + Q_{(n+2)/2}}{2} & \text{if } n \text{ is even} \end{cases} \quad \text{(B2)}$$

Very similar to the MK approach, a positive or negative value of Q_{sen} respectively indicates the presence of a positive or a negative trend, and its value represents the steepness of the trend.

A step-by-step procedure for formal detection and attribution analysis is described below by considering OND T_{max}. The following steps are repeated for each considered variable, viz. Annual T_{max}, JF T_{max}, MAM T_{max}, JJAS T_{max}, OND T_{max}, Annual T_{min}, JF T_{min}, MAM T_{min}, JJAS T_{min} and OND T_{min}, separately.

Appendix 3. Step-by-step procedure for formal detection and attribution analysis

Step 1. Calculation of signal strength (S) for observation and all model simulations from different experiments (piControl, historical, historicalNat, historicalGHG and historicalMisc) using Eq. (1). Fingerprint $F(x)$ is the leading EOF of the ensemble-averaged 9 OND T_{max} time series obtained from historical simulations (9 models for T_{max} as shown in Table 2).

Step 2. In this step, we check whether the variability observed in OND T_{max} is similar to the variability of OND T_{max} in piControl simulations. As discussed in Section 3, a Monte Carlo test is adopted to estimate the likelihood of observations being drawn from the control distribution (piControl simulations). For the observed time series length, n is 56 and for the control simulation length, m is 6276 (combination of all piControl model simulation in case of T_{max}). Groups of non-overlapping p members ($p = 1$ for observation, $p = 3$ for historicalNat) of length n are randomly selected from m years of 'piControl' simulations. Ensemble averaged p members are used to calculate control S.

This process is repeated 10 000 times to obtain a distribution of control S. If the observed S falls beyond the range of control S distribution at the 5% significance level, then it can be claimed that a human influence on climate is discernible and the changes are unnatural. The results indicate that S of observed OND T_{max} is statistically different from control S distribution.

This process is repeated to check the likelihood of historical simulations of OND T_{max} statistically being drawn from control simulations using a Monte Carlo test.

Step 3. After successful detection, attribution is addressed by comparing the observed S with that obtained from different experimental simulations such as historical, historicalNat, historicalGHG and historicalMisc. For comparison, S from each model and MMM simulations obtained from different experiments and their 95% confidence interval are plotted along with observed S.

Step 4. For unequivocal attribution, the observed S should be consistent with the S of the historical simulation (representing anthropogenic forcing) and simultaneously inconsistent with the S of the historicalNat simulation (which represents solar and volcanic forcing). Comparison of S for OND T_{max} from different experiments is shown in Fig. 4.

Editorial responsibility: Eduardo Zorita, Geesthacht, Germany

Submitted: November 22, 2016; Accepted: July 9, 2018
Proofs received from author(s): September 9, 2018